Journal of Solid State Chemistry 184 (2011) 1048–1053

Contents lists available at ScienceDirect

Journal of Solid State Chemistry

journal homepage: www.elsevier.com/locate/jssc

Mild hydrothermal synthesis and ferrimagnetism of $Pr_3Fe_5O_{12}$ and $Nd_3Fe_5O_{12}$ garnets

Li Guo, Keke Huang, Yan Chen, Guanghua Li, Lin Yuan, Wen Peng, Hongming Yuan*, Shouhua Feng

State Key Laboratory of Inorganic Synthesis and Preparative Chemistry, Jilin University, 130012 Changchun, PR China

ARTICLE INFO

Article history:
Received 29 November 2010
Received in revised form
28 February 2011
Accepted 5 March 2011
Available online 15 March 2011

Keywords:
Hydrothermal
Garnet
Ferrimagnetism

ABSTRACT

Two pure light rare earth iron garnets $Pr_3Fe_5O_{12}$ and $Nd_3Fe_5O_{12}$ single crystals were synthesized under mild hydrothermal conditions and structurally characterized by single crystal and powder X-ray diffraction methods. Both compounds crystallize in cubic space group $Ia\bar{3}d$ with lattice parameters $a=12.670(2)$ Å for $Pr_3Fe_5O_{12}$ and $a=12.633(2)$ Å for $Nd_3Fe_5O_{12}$, respectively. The synthesis of compounds was studied with regard to phase evolution and morphology development with hydrothermal conditions. We proposed the formation mechanisms and formulated a reasonable explanation for their growth habits. Ferrimagnetic Curie temperatures which have been inferred from thermomagnetization curves were 580 K for $Pr_3Fe_5O_{12}$ and 565 K for $Nd_3Fe_5O_{12}$, and the transitions of long range order were also evidenced by differential scanning calorimetry method. The result of magnetic properties has shown that moments of the large radius Pr^{3+} and Nd^{3+} ions are parallelly coupled with net moments of iron ions.

© 2011 Elsevier Inc. All rights reserved.

1. Introduction

Rare earth iron garnets with narrow ferromagnetic resonance linewidths, very low hysteresis losses, and excellent dielectric properties have been widely applied in microwave devices in a wide range of frequencies (1–100 GHz) and typically employed as magnetic recording media [1–3]. The rare earth iron garnets which can be described by chemical unit formula $RE_3Fe_5O_{12}$ belong to cubic system with space group $Ia\bar{3}d$, whose cell contains eight $RE_3Fe_5O_{12}$ molecules and crystal lattice contains three crystallographic sites, dodecahedral site 24*c* {RE^{3+}}, octahedral site 16*a* [Fe^{3+}] and tetrahedral site 24*d* (Fe^{3+}) [4,5]. The garnet in fact does not allow distortion to lower symmetry owing to its non-efficiently packed structure [6], which makes iron garnet structure become unstable with increasing rare earth ionic radius. In 1961, Geller [7] and Espinosa [8] have concluded that the maximum lattice parameter for unsubstituted rare earth iron garnets obtained through conventional sintering method could not be greater than 12.540 Å. A reasonable explanation based on the free energy calculations for the high temperature solid state reaction was given by Kimizuka et al. in 1983[9]. The large radius Pr^{3+} and Nd^{3+} have been expected to fill dodecahedra *c* site in an iron garnet, but in most cases, they may be mixed with smaller ions such as Y^{3+}, Bi^{3+} and rare earth ions from Lu to Sm [10–17]. Recently, Gomi [10] and Yang [11], respectively, employed the RF sputtering and sol–gel method to produce $Pr_xY_{3-x}Fe_5O_{12}$ and $Nd_xY_{3-x}Fe_5O_{12}$ garnets, and extended Pr^{3+} and Nd^{3+} substitution limit up to 2.0.

Ferrimagnetism has been found in the garnets [18]. In most cases, the Fe^{3+} ions form two nonidentical sublattices in up and down spin states, and the rare earth ion causes the formation of a third sublattice, then the three sublattices result in a net non-zero magnetization in material. In rare earth iron garnets, there is a strong interaction between the two sublattices occupied by Fe^{3+} ions, and therefore, the iron ions alone dominate the ferromagnetic order since the coupling between the rare earth and iron ions is relatively weak [2]. Much work on magnetic behaviors of the heavier rare earth iron garnets, in which different non-magnetic ions replace the iron or rare earth ions, has been reviewed by Geller [6].

The researchers have attempted to break the limitation mentioned above to the synthesis of pure praseodymium or neodymium iron garnets. However, a rigorous literature search reveals that few papers devoted to the study of $Pr_3Fe_5O_{12}$ and $Nd_3Fe_5O_{12}$ exist. It has been reported that Fratello et al. have synthesized successfully praseodymium and neodymium iron garnets by liquid phase epitaxy (LPE) on $Sm_3(ScGa)_5O_{12}$ substrates at about 875 and 900 °C [19,20]. By synchrotron radiation study, Komori recently determined the crystal structures of the above synthesized compounds [21,22]. In LPE process, perovskite orthoferrite as a primary phase grows on the substrate, the lattice constants of samples and substrates need to match exactly, and the impurities of Pb and Pt could be embedded in the sites of the lattices. Until now few experimental results unambiguously reveal ferrimagnetic properties of pure praseodymium and neodymium iron garnets, although some

* Corresponding author. Fax: +86 431 85168624.
E-mail address: hmyuan@mail.jlu.edu.cn (H. Yuan).

0022-4596/$ - see front matter © 2011 Elsevier Inc. All rights reserved.
doi:10.1016/j.jssc.2011.03.010

theoretical predictions and calculations about them have been reported [23,24]. In the present work we will describe the hydrothermal synthesis and ferrimagnetic behaviors of $Pr_3Fe_5O_{12}$ and $Nd_3Fe_5O_{12}$.

2. Experimental section

2.1. Synthesis

The samples were prepared by mild hydrothermal method and crystallization took place in a Teflon-lined stainless steel autoclave (ca. 18 cm^3 capacity) with a filling capacity of 80%. The starting materials were Fe $(NO_3)_3 \cdot 9H_2O$ (AR), $Pr(NO_3)_3 \cdot 6H_2O$ (AR) and $Nd(NO_3)_3 \cdot 6H_2O$ (AR) and KOH(AR). In order to ensure intimate mixing of reagents, 0.4 mol/L solutions of the metal salts were prepared. KOH pellets were employed as mineralizer. A typical synthesis was as following: 3 ml Pr $(NO_3)_3$ or Nd $(NO_3)_3$ was mixed with 5 ml Fe $(NO_3)_3$ solution at room temperature. Then the mixture was stirred for 30 min to form the dispersed solution. A cloudy precipitate was observed in the solution once KOH is added. After adding 20 g KOH, the mixture was stirred to form brown slurry before being transferred into Teflon-lined stainless steel autoclave to complete crystallization under autogenous pressure at 260 °C for 10 days. After the autoclave was naturally cooled and depressurized, the resulting black single crystals $Pr_3Fe_5O_{12}$ ($Nd_3Fe_5O_{12}$) were collected by filtration, washed with deionized water and finally dried in air at ambient temperature.

2.2. Characterization

Product compositions were determined by inductively coupled plasma spectroscopy (ICP) as well as energy dispersive spectroscopy (EDS). The powder X-ray diffraction data was collected on Rigaku D/Max 2500V/Pc X-ray diffractometer with Cu$K\alpha$ radiation ($\lambda = 1.5418$ Å) at 50 KV and 200 mA at room temperature. The step scanning in the angle range of $15^\circ \le 2\theta \le 80^\circ$ and increments of 0.02° were employed. The morphology of the products was checked with a JEOL JSM-6700F scanning electron microscope (SEM). The temperature dependence of magnetic moments from 300 to 673 K was measured using a Lake shore 7407 vibrating sample magnetometer (VSM) under applied field of 100 Oe, while zero-field cooled (ZFC) and field cooled (FC) curves were recorded in an applied field 100 Oe from 4 to 300 K by Quantum Design MPMS-XL (SQUID). Hysteresis loops for different temperatures were also recorded by SQUID in an applied magnetic field up to 3 T. Moreover, measurements of differential scanning calorimetry (DSC) were performed in a temperature range from 450 to 650 K at a scanning rate of 10 K/min under protecting N_2.

2.3. X-ray crystallography

The data collection and the structural analysis were performed on a Rigaku RAXIS-RAPID single-crystal diffractometer equipped with a fine-focus, 5.4 KW sealed-tube X-ray source (graphite-monochromatized Mo$K\alpha$ radiation with $\lambda = 0.71073$ Å) at 293(2) K for $Pr_3Fe_5O_{12}$ and $Nd_3Fe_5O_{12}$. The diffraction data were collected at room temperature by the ω-scan method. The data processing was accomplished with the PROCESS-AUTO processing program. Direct methods were used to solve the structure using the SHELXL crystallographic software package. All atoms were easily found from the difference Fourier map and refined anisotropically. Crystal parameters and details of the data collection and refinement of the two compounds are listed in Table 1. Atomic coordinates, selected bond lengths and angles, and anisotropic displacement parameters are listed in Table S1–6.

3. Results and discussion

3.1. Composition, morphology and structure description

The fantastic properties of rare earth iron garnets require higher quality crystals for more experimental and theoretical work. References [19,20] state that their samples have been synthesized via the LPE method and the samples had Pb and Pt inclusion from the crucible and flux. The inclusion cannot be avoided for that LPE method needs PbO flux and high temperature and the Pb can affect some physical properties, for example, increase the optical absorption coefficient [25]. In addition, the method is very complicated and hard-handling. Here we developed the hydrothermal synthesis which provides a promising route to prepare well-crystalline and phase-pure $RE_3Fe_5O_{12}$ (RE=Pr, Nd) in one-step in a tightly closed

Table 1
Crystal data and structure refinement for $RE_3Fe_5O_{12}$ (RE=Pr, Nd).

Empirical formula	$Pr_3Fe_5O_{12}$	$Nd_3Fe_5O_{12}$
Formula weight	893.98	903.97
Temperature (K)	293(2)	293(2)
Wavelength (Å)	0.71073	0.71073
Crystal system, space group	Cubic, $Ia\bar{3}d$	Cubic, $Ia\bar{3}d$
Unit cell dimensions (Å)	a=12.670(2)	a=12.633(2)
Volume (Å^3)	2033.7(4)	2015.9(4)
Z, Calculated density (Mg/m^3)	8, 5.840	8, 5.957
Absorption coefficient (mm^{-1})	21.062	21.062
F(0 0 0)	3224	3248
Crystal size (mm^3)	0.12 × 0.12 × 0.12	0.12 × 0.12 × 0.12
Theta range for data collection (deg.)	3.94–27.44	3.95–27.31
Limiting indices	$-16 \le h \le 16$ $-16 \le k \le 16$ $-15 \le l \le 16$	$-16 \le h \le 16$ $-16 \le k \le 16$ $-16 \le l \le 16$
Reflections collected/unique	8517/199 [R(int)=0.0358]	8382/197 [R(int)=0.0320]
Completeness to theta=27.44	99.0%	100.0%
Refinement method	Full-matrix least-squares on F^2	Full-matrix least-squares on F^2
Data/restraints/parameters	199/0/17	197/6/17
Goodness-of-fit on F^2	1.292	1.329
Final R indices[$I > 2$sigma(I)]	R_1=0.0220, wR_2=0.0568	R_1=0.0245, wR_2=0.0595
R indices(all data)	R_1=0.0233, wR_2=0.0577	R_1=0.0247, wR_2=0.0595
Largest diff. peak and hole (Å^{-3})	0.554 and −1.419e	0.726 and −1.483e

vessel. Compositional analyses of hydrothermal samples by ICP and EDS gave a formula $RE_3Fe_5O_{12}$ (RE=Pr, Nd). The ICP composition analysis indicates that the ratio of RE:Fe is in good agreement with the theoretical value for the garnet type oxides. Fig. S1 gives EDS analysis of selected regions for the sample, and the analysis confirms that RE:Fe ratio in the sample is 3:5, consistent with the ICP result, and samples do not contain any other non-component elements. The powder X-ray diffraction patterns which agree well with the ones that were simulated on basis of the single crystal structure (Fig. 1a and c) are shown in Fig. 1b and d. Based on the powder XRD analysis, it can be concluded that the crystals are well crystallized and without detectable impure phase. Fig. 2 shows the scanning electron micrographs (SEM) images of the title compounds, it can be seen the two compounds obtained by hydrothermal approach are crystalline with a uniform rhombic dodecahedron shape. Deduced from the single crystal X-ray diffraction analysis, both $Pr_3Fe_5O_{12}$ and $Nd_3Fe_5O_{12}$, which are isomorphic compounds, crystallize in the cubic symmetry space group $Ia\bar{3}d$ with garnet structure and the lattice constants are 12.670(2) and 12.633(2) Å, respectively. The garnet structure is illustrated in Fig. 3. The FeO_4 tetrahedron and FeO_6 octahedron are linked together by corners. The Pr and Nd atoms are coordinated by eight O atoms in distorted dodecahedral geometry. The REO_8 dodecahedra shares edges with adjacent FeO_6 octahedrons.

3.2. Crystal growth condition

Hydrothermal crystallization is a ready process but many factors influencing the formation of products are involved, such as alkalinity, reaction time, crystallization temperature. In order to develop a practical synthesis procedure, we need to look at some synthetic factors. The KOH not only acts as mineralizing agent but also maintains the alkalinity which plays an important role in governing the formation of $RE_3Fe_5O_{12}$ (RE=Pr, Nd) crystals. Here a dissolution-precipitation mechanism, by which amorphous precursors dissolved into solution to form complex groups which would crystallize into crystal by dehydrating water, was proposed for hydrothermal reactions. Taking $Pr_3Fe_5O_{12}$ as an example, the effect of alkalinity on the preparation was investigated in the presence of different amount of KOH with temperature and time being fixed at 260 °C and 10 days. After adding KOH, Pr^{3+} and Fe^{3+} ions precipitate and form amorphous $Pr(OH)_3$ and $Fe(OH)_3$. Then the amorphous $Pr(OH)_3$ and $Fe(OH)_3$ dissolved in solution could form hydroxyl-complexes groups, such as $Pr(OH)_4^-$ and $Fe(OH)_4^-$ in basic solution, which may act as the crystal growth units and dehydrate to form nuclei of a phase. The degree of dissolution depends on the solubility of each material established at a given hydrothermal condition. As can be concluded from the experimental results, the reaction is very sensitive to the amount of KOH. When the amount of KOH is less than 9 g, the amorphous $Pr(OH)_3$ and $Fe(OH)_3$ are almost not to be dissolved and thus crystallized as precipitation $Pr(OH)_3$ and Fe_2O_3 after hydrothermal treatment. When it is added to 9–12 g, amorphous $Pr(OH)_3$ and $Fe(OH)_3$ dissolved in a hydrothermal environment, but the solubility is insufficient, thus liquid and solid boundary get a nonstoichiometric

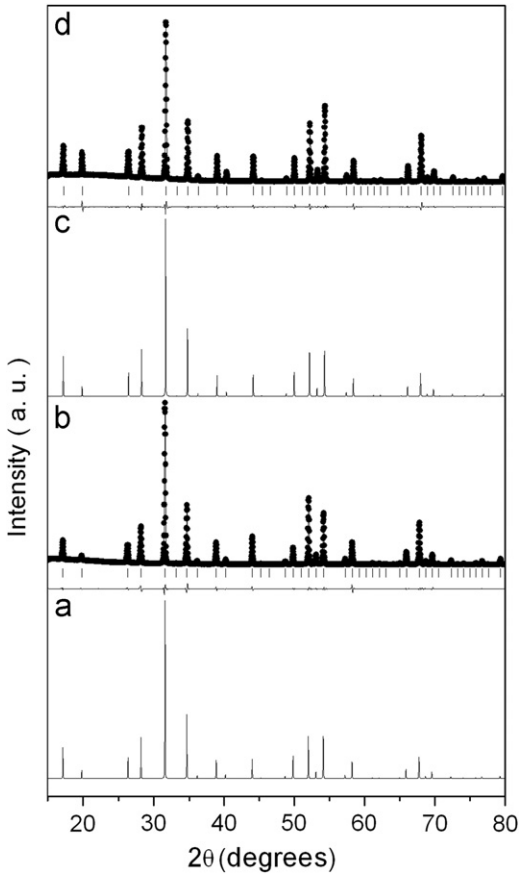

Fig. 1. XRD patterns of single crystal simulated (a, c) and powder refinement (b, d) for $Pr_3Fe_5O_{12}$ and $Nd_3Fe_5O_{12}$, respectively.

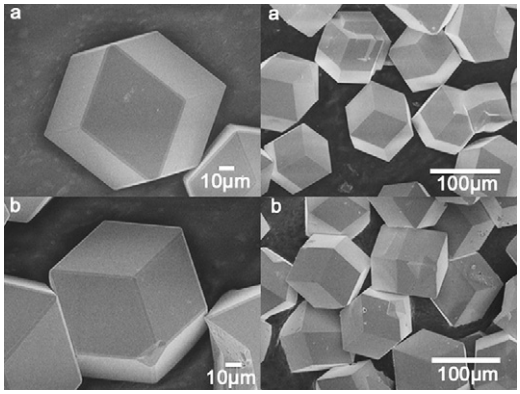

Fig. 2. SEM photographs of $Pr_3Fe_5O_{12}$ (a) and $Nd_3Fe_5O_{12}$ (b) single crystals.

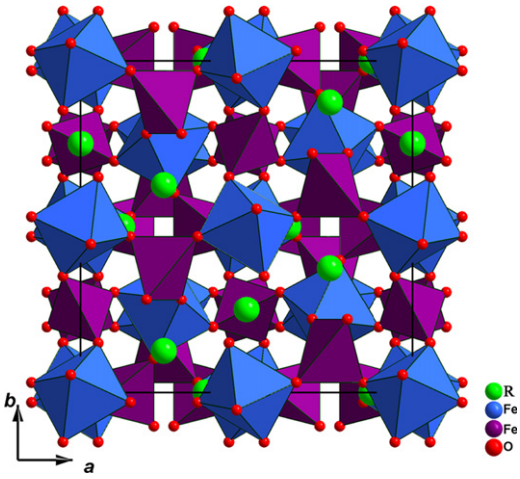

Fig. 3. The structure of $RE_3Fe_5O_{12}$ (RE=Pr, Nd). Small red and large green spheres represent O and R atoms, respectively. Blue octahedron and purple tetrahedron represent FeO_6 and FeO_4 units, respectively. (For interpretation of the references to color in this figure legend, the reader is referred to the web version of this article.)

proportion to form main phase $PrFeO_3$ (Fig. 4a) by dehydration. When it further reaches 12 g, the $Pr_3Fe_5O_{12}$ nucleation would favorably be formed due to sufficient solubility of Pr and Fe sources, so this amount is the minimum to form pure $Pr_3Fe_5O_{12}$. When it gradually increases until the KOH cannot be dissolved (20 g), the product is always the $Pr_3Fe_5O_{12}$, but corresponding sizes change from about 1 μm (Fig. 4b) to 120 μm, which can be ascribed to that high KOH concentration induced growth rate predominate over the nucleation rate in hydrothermal solutions. Thus, the pure single crystals can only be synthesized when alkaline concentrations are high enough.

To investigate the formation mechanism of the $Pr_3Fe_5O_{12}$, the effects of different reaction temperatures and time were investigated with the amount of KOH being fixed at 20 g. The experimental results show that when the reaction temperature is below 200 °C, the $Pr_3Fe_5O_{12}$ cannot be formed, and when it is above 200 °C, the corresponding reaction time decreases with temperature increasing. This can be explained by that Kinetics and Thermodynamics are related to each other in ways. The analysis has shown that the pure phase $Pr_3Fe_5O_{12}$ can be obtained at 260 °C when the hydrothermal treatment is carried out after short time (1 day), but the corresponding particle size is small and crystal quality is bad (Fig. 4c). The effect of different reaction temperatures on the formation of crystalline $Pr_3Fe_5O_{12}$ was also investigated when the reaction time and KOH were fixed at 10 days and 20 g. The experimental results show that the pure phase $Pr_3Fe_5O_{12}$ can still be obtained when reaction temperature is as low as 200 °C. Similarly, both the corresponding particle size and crystal quality reduce (Fig. 4d). The sizes of crystals become larger with temperature and time increasing, and crystal quality gradually becomes better with increasing size. When temperature and time, respectively, exceed 260 °C and 10 days, both the size and quality will remain unchanged. Whatever kinds of rare earth (Pr and Nd) are used in experiment, similar phenomena can always be observed, but for $Nd_3Fe_5O_{12}$, the above minimum time and temperature are 1.5 days and 220 °C.

The gorgeous single crystal $RE_3Fe_5O_{12}$ (RE=Pr, Nd) with about 120 μm size is crystallized in the solution containing 20 g KOH at 260 °C for 10 days under straightforward hydrothermal condition.

3.3. Magnetic properties

Compared with the earlier magnetic studies [19,20], our data is more complete (ZFC and FC curves are added, the hysteresis loops are measured and applied to determine saturation magnetization Ms). Furthermore, the measured temperature range was extended and low field for thermo-magnetization curves and high field for hysteresis loops were applied. We expanded on the details of magnetic studies and discussed the effect of the external magnetic field on the Curie temperature. The compensation point was also considered. Therefore, the results are relatively more particular and abundant.

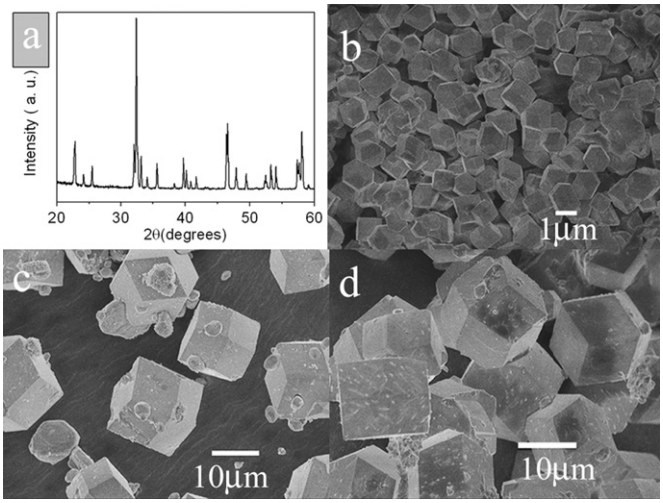

Fig. 4. XRD pattern and SEM photographs under different hydrothermal conditions: (a) 9–12 g KOH, 260 °C and 10 days, (b)12 g KOH, 260 °C and 10 days, (c) 20 g KOH, 260 °C and 1 day, and (d) 20 g KOH, 200 °C and 10 days.

The strongest super-exchange interactions occur in Fe^{3+} (a)–O^{2-}–Fe^{3+} (d) in all iron garnets, therefore, garnets possess almost the approximate Curie temperatures, about 560 K [26]. Actually, the magnitudes of the super-exchange interactions depend strongly on the angles between iron ions. The Pr^{3+} and Nd^{3+} ionic radius (1.14 and 1.12 Å) are large enough to lead to a great change of the bond lengths and angles compared with those of heavier rare earth iron garnets. As can be seen from the crystallographic data, the angles of Fe^{3+} (a)–O^{2-}–Fe^{3+} (d) are 129.2° for $Pr_3Fe_5O_{12}$ and 128.6° for $Nd_3Fe_5O_{12}$. These values are slightly larger than those of heavier rare earth iron garnets, such as 126.6° for $Y_3Fe_5O_{12}$ and 127.4° for $Gd_3Fe_5O_{12}$ [27]. Therefore, in $Pr_3Fe_5O_{12}$ and $Nd_3Fe_5O_{12}$, the coupling between the two sublattices occupied by Fe^{3+} ions should be stronger, since the coupling increases with increasing angle of Fe^{3+} (a)–O^{2-}–Fe^{3+} (d). Furthermore, the angle is proportional to the radius of rare earth ions. Experimentally, ferrimagnetic ordering temperatures of rare earth iron garnets from $Lu_3Fe_5O_{12}$ to $Sm_3Fe_5O_{12}$ have been found to gradually rise with increasing of ionic radius of the rare earth [28]. Thus we expect that the ferrimagnetic ordering temperature rises when c sites are fully occupied by Pr^{3+} or Nd^{3+} ions. The transition temperature from ferromagnetic to paramagnetic state is called the Curie point. In our experiment, the thermo-magnetization curves for present compounds were measured under applied field of 100 Oe over 300–673 K by VSM, and displayed in Fig. 5. The Curie points derived from point of intersection of maximum slope tangent to the curve with temperature axis were 580 and 565 K for $Pr_3Fe_5O_{12}$ and $Nd_3Fe_5O_{12}$, respectively. Usually, a magnetic contribution to the specific heat can be expected, since from paramagnetic to ferromagnetic state, the transition is of second-order phase and associated with entropy change. At Curie temperature, each of the compounds ($Y_3Fe_5O_{12}$ as reference) has shown a visible variation in the heat flow curves as a function of the temperature (Fig. 6), which evidenced the change of the long range order. The value difference through two methods is originated from external field. If we get rid of the effect of the external magnetic field on the measured values, the results, obtained by DSC and VSM, could be almost the same. These Curie points are not significantly higher than those of others rare earth iron garnets studied earlier [28] and $Y_3Fe_5O_{12}$. On the one hand this might be explained by little contribution of rare earth ions to spontaneous magnetization at temperature close to the Curie point. On the other hand, a possible reason is the presence of non-collinear magnetic structure in the magnetic sublattices, such as triangular spins configurations so-called Yafet–Kittel types [29] or spiral configurations.

For the heavier rare earth ions, moment and spin are related by a negative g factor [23]. Therefore, the total iron sublattices and the c sublattice are antiferromagnetically coupled by the super-exchange interaction via the intervening O^{2-} ions. In 1960, Wolf theoretically pointed out that the rare earth ions Ce^{3+}, Pr^{3+}, and Nd^{3+} corresponding to positive g factor will result in parallel ordering of magnetic moments between Pr^{3+} or Nd^{3+} and the net Fe^{3+} ion moments [23]. In some cases of Pr^{3+} or Nd^{3+} substituting Y^{3+} in yttrium iron garnets, the main purpose was to determine the magnetic behaviors of Pr^{3+} or Nd^{3+} ions and to extrapolate to the possible magnetic properties of $Pr_3Fe_5O_{12}$ or $Nd_3Fe_5O_{12}$. As discussed above, Wolf reasonably explained that the increasing of magnetic moment of yttrium–neodymium iron garnet at room

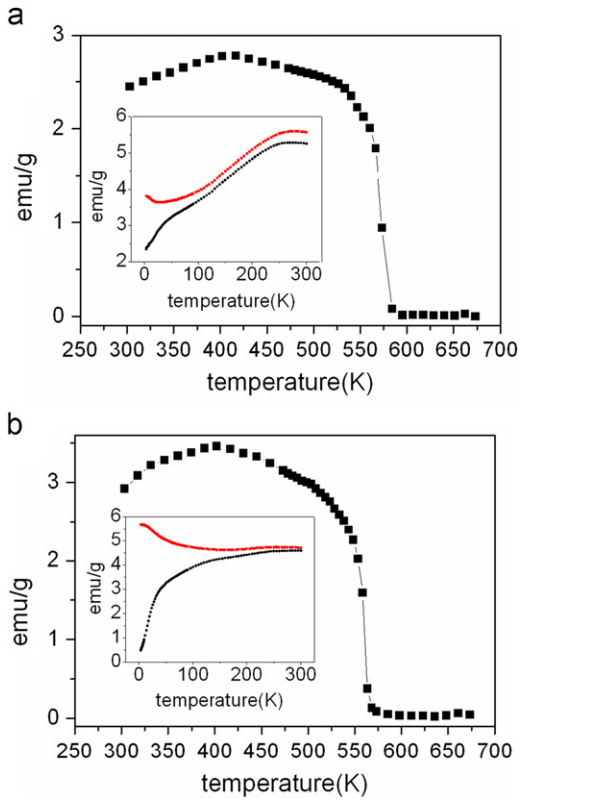

Fig. 5. Variation of magnetization as a function of temperature for $Pr_3Fe_5O_{12}$ (a) and $Nd_3Fe_5O_{12}$ (b) at H=100 Oe in temperature range of 300–673 K. Inset: temperature dependence of ZFC (black color curve) and FC (red color curve) magnetization for $Pr_3Fe_5O_{12}$ (a) and $Nd_3Fe_5O_{12}$ (b) under 100 Oe over 4–300 K. (For interpretation of the references to color in this figure legend, the reader is referred to the web version of this article.)

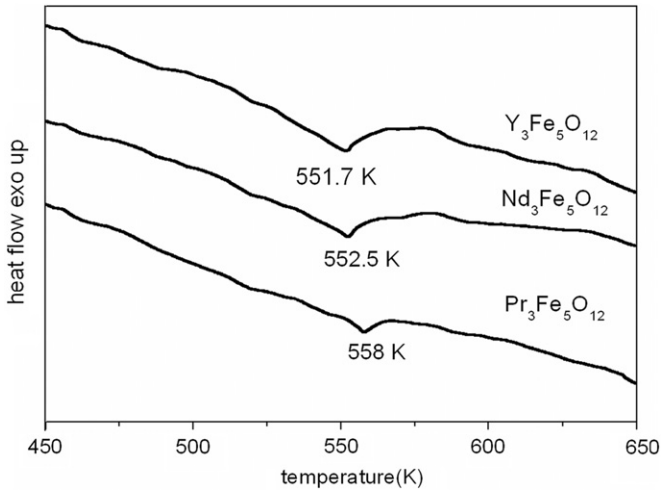

Fig. 6. DSC curves of $RE_3Fe_5O_{12}$ (RE=Pr, Nd) and $Y_3Fe_5O_{12}$.

temperature was due to the positive contribution of Nd ion. Hysteresis loops of the $RE_3Fe_5O_{12}$ (RE=Pr, Nd) at 4, 100 and 300 K were also recorded, and the results are presented in Fig. 7. The observed coercive forces are 76 Oe for $Pr_3Fe_5O_{12}$ and 381 Oe for $Nd_3Fe_5O_{12}$ at 4 K, while they are 5 and 28 Oe at 100 K. Their coercive forces have not been observed at room temperature. In the present case the saturation magnetization values for the $Pr_3Fe_5O_{12}$ and $Nd_3Fe_5O_{12}$ are 23.75 and 21.98 emu/g at 300 K, respectively. When converted to units of Bohr magneton, they are slightly higher than

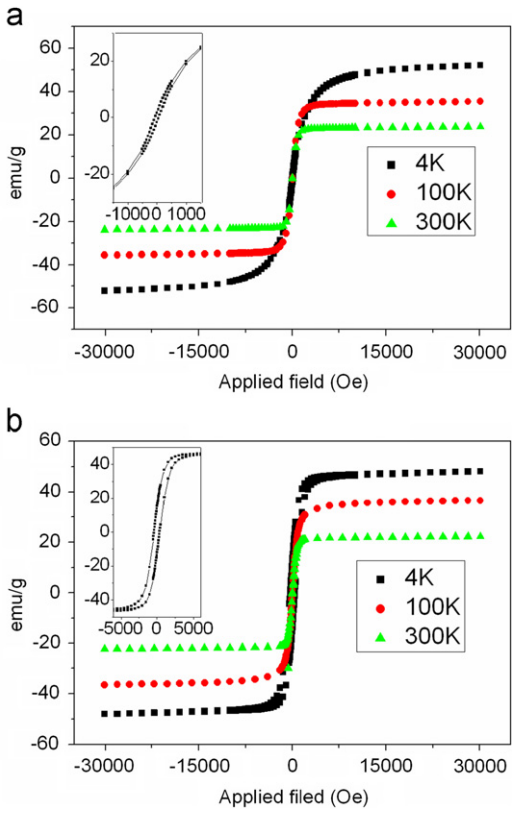

Fig. 7. Hysteresis loops of $Pr_3Fe_5O_{12}$ (a) and $Nd_3Fe_5O_{12}$ (b) at an applied field up to H=3 T at different temperature of 4, 100 and 300 K. The insets show the expanded scale of 4 K.

that of $Y_3Fe_5O_{12}$ (26 emu/g for bulk $Y_3Fe_5O_{12}$ [30]), which is more obvious at lower temperatures [31]. Thus Pr^{3+} or Nd^{3+} ion moment is parallel to the resultant moments of the irons sublattices, and our experimental results are also consistent with theoretical expectation of light rare earth iron garnets.

The main feature of ferrimagnetic behaviors of some garnets is that they exhibit compensation temperatures where magnetic moment falls to zero and recovers. At compensation point, the magnetic moment of rare earth sublattice is quantitatively equal to the resultant moment of iron sublattices. Therefore, the compensation temperature depends on the magnitude and direction of the magnetic moment of rare earth sublattice. Obviously, the compensation points for title compounds have not been observed in the whole experimental temperature range (Fig. 5). The disappearance of compensation temperatures for $Pr_3Fe_5O_{12}$ and $Nd_3Fe_5O_{12}$ further demonstrates that Pr^{3+} or Nd^{3+} ion moments are parallel to the resultant moment of the two iron ions sublattices, and also provides a direct confirmation of Wolf's prediction.

4. Conclusions

We have fortunately prepared two pure light rare earth iron garnets, $Pr_3Fe_5O_{12}$ and $Nd_3Fe_5O_{12}$, under mild hydrothermal condition. The hydrothermal synthesis technique for transition metal oxides is promising in the preparation of complex oxides in terms of relatively low reaction temperature, one-step synthesis procedure, easy handling and controllable particle size. The alkalinity, reaction temperature and reaction time of the system play key roles in influencing the crystallization and composition of the products. The larger radius ion occupies c sites, leading to

the expansion of the volumes of the title compounds and the change of bond lengths and angles of iron ions surrounded by O atoms. For Pr^{3+} and Nd^{3+} ion, the ion with positive g factor induces a parallel moment between two iron ions and one rare earth ion, hence results in disappearance of compensation point. This parallel coupling is a more general phenomenon in title compounds.

Acknowledgments

This work was supported by the National Natural Science Foundation of China (Nos. 90922034 and 20771042).

Appendix A. Supplementary Information

Further details of the crystal structure investigation(s) may be obtained from Fachinformationszentrum Karlsruhe, 76344 Eggenstein-Leopoldshafen, Germany (fax: (+49)7247 808 666; e-mail: crysdata@fiz-karlsruhe.de, http://www.fiz-karlsruhe.de/request_for_deposited_data.html) on quoting the appropriate CSD number 422690-422691. Other Supplementary data associated with this article can be found in the online version at: doi:10.1016/j.jssc.2011.03.010.

References

[1] M. Sugimoto, J. Am. Ceram. Soc. 82 (1999) 269.
[2] Ü. Özgür, Y. Alivov, H. Morkoc, J. Mater. Sci.—Mater. El 20 (2009) 789.
[3] Ü. Özgür, Y. Alivov, H. Morkoc, J. Mater. Sci.—Mater. El 20 (2009) 911.
[4] M.A. Gilleo, S. Geller, Phys. Rev. 110 (1958) 73.
[5] S. Geller, Z. Kristallogr., Bd. 125 (1967) 1.
[6] S. Geller, J. Appl. Phys. 31 (1960) 30S.
[7] S. Geller, H.J. Williams, R.C. Sherwood, Phys. Rev. 123 (1961) 1692.
[8] G.P. Espinosa, J. Chem. Phys. 37 (1962) 2344.
[9] N. Kimizuka, A. Yamamoto, H. Ohashi, T. Sugihara, T. Sekine, J. Solid State Chem. 49 (1983) 65.
[10] M. Gomi, H. Toyoshima, J. Appl. Phys. 82 (1997) 1359.
[11] Z.J. Cheng, H. Yang, J. Mater. Sci.—Mater. El 18 (2007) 1065.
[12] S. Geller, H.J. Williams, R.C. Sherwood, J.P. Remeika, G.P. Espinosa, Phys. Rev. 131 (1963) 1080.
[13] K. Jawahar, Banarji Behera, R.N.P. Choudhary, J. Mater. Sci.—Mater. El. 20 (2009) 872.
[14] K. Nagashio, J. Am. Ceram. Soc. 89 (2006) 1504.
[15] K. Nagashio, K. Kuribayashi, J. Am. Ceram. Soc. 90 (2007) 238.
[16] L.M. Yu, J.J. Wang, S.X. Cao, S.J. Yuan, J.C. Zang, J. Mater. Sci. 42 (2007) 5335.
[17] Antonio Azevedo, C. Cinbis, M.H. Kryder, J. Appl. Phys. 74 (1993) 7450.
[18] S. Geller, M.A. Gilleo, Acta. Crystallogr. 10 (1957) 239.
[19] V.J. Fratello, C.D. Brandle, S.E.G. Slusky, A.J. Valentino, M.P. Norelli, R. Wolfe, J. Crys., Growth 75 (1986) 281.
[20] S.E.G. Slusky, J.F. Dillon Jr., C.D. Brandle, M.P. Norelli, V.J. Fratello, Phys. Rev. B 34 (1986) 7918.
[21] T. Komori, T. Sakakura, Y. Takenaka, K. Tanaka, T. Okuda, Acta Crystallogr. E 65 (2009) sup 1–5.
[22] T. Komori, T. Sakakura, Y. Takenaka, K. Tanaka, T. Okuda, Acta Crystallogr. E 65 (2009) sup 1–5.
[23] W.P. Wolf, J. Appl. Phys. 32 (1961) 742.
[24] Xavier Oudet, J. Magn. Magn. Mater. 272 (2004) 562.
[25] Qing-Hui Yang, Huai-Wu Zhang, Ying-Li Liu, Qi-Ye Wen, Jie Zha, Chin. Phys. Lett 25 (2008) 3957.
[26] R. Pauthenet, J. Appl. Phys. 30 (1959) 290S.
[27] R.J. Joseyphus, A. Narayanasamy, A.K. Nigam, R. Krishnan, J. Magn. Magn. Mater. 296 (2006) 57.
[28] S.C. Parida, S.K. Rakshit, Ziley Singh, J. Solid. State. Chem. 181 (2008) 101.
[29] Y. Yafet, C. Kittel, Phys. Rev. 87 (1952) 290.
[30] P. Vaqueiro, M.A. López-Quintela, J. Rivas, J.M. Greneche, J. Magn. Magn. Mater. 169 (1997) 56.
[31] E. Garskaite, K. Gibson, A. Leleckaite, J. Glaser, D. Niznansky, A. Kareiva, H. Meyer, J. Chem. Phys. 323 (2006) 204.